Article

Intrinsic Effect of Pyridine-N-Position on Structural Properties of Cu-Based Low-Dimensional Coordination Frameworks

Anna Walczak [1,2,†]**, Gracjan Kurpik** [1,2,†] **and Artur R. Stefankiewicz** [1,2,*]

[1]   Faculty of Chemistry, Adam Mickiewicz University, Uniwersytetu Poznańskiego 8, 61-614 Poznań, Poland; anna.jenczak@amu.edu.pl (A.W.); grakur@amu.edu.pl (G.K.)

[2]   Center for Advanced Technologies, Uniwersytetu Poznańskiego 10, 61-614 Poznań, Poland

*   Correspondence: ars@amu.edu.pl

†   These authors contributed equally to this work.

check for updates

Abstract: Metal-organic assemblies have received significant attention for catalytic and other applications, including gas and energy storage, due to their porosity and thermal/chemical stability. Here, we report the synthesis and physicochemical characterization of three metallosupramolecular assemblies consisting of isomeric ambidentate pyridyl-β-diketonate ligands L1–L3 and Cu(II) metal ions. It has been demonstrated that the topology and dimensionality of generated supramolecular aggregates depend on the location of the pyridine nitrogen donor atom in L1–L3. This is seen in characterization of two distinct 2D polymeric assemblies, i.e., $[Cu(L1)_2]_n$ and $[Cu(L2)_2]_n$, in which both β-diketonate and pyridine groups are coordinated to the Cu(II) center, as well as in characterization of the mononuclear 1D complex $Cu(L3)_2$, in which the central atom is bound only by two β-diketonate units.

1. Introduction

Coordination-driven self-assembly processes harness the directionality and reversibility of metal–ligand interactions to allow formation of supramolecular architectures with strictly defined shape and topology [1–6]. The spontaneous but controlled generation of well-defined multimetallic architectures is seen in the formation of one-, two- and three-dimensional coordination polymers (CPs) with numerous applications in, e.g., magnetism, molecular separations, dye degradation and catalysis [7–9]. The great advantage of CPs over other types of supramolecular materials is their facile chemical modification by changing, e.g., the position/type of donor atoms or metal ion coordination geometry. By combining appropriate metal cations with carefully selected organic linkers (ligands), the structural properties and topology of CPs can be easily modulated and adapted to a desired function, e.g., in catalysis or sorption/separation processes [10,11].

Coordination complexes containing ambidentate ligands that are capable of binding metal-ion centres in more than one way through different donor-atom combinations provide an efficient strategy in the construction of functional coordination assemblies [12,13]. Of the many structurally distinct ambidentate ligands, pyridyl-β-diketonates have been widely employed in the generation of different coordination systems from simple mononuclear complexes, [14] through cages [15] and macrocycles [16] to larger architectures (e.g., polymers (CPs) and metal-organic frameworks) [15,17–23] Importantly, coordination structures based on ambidentate ligands have shown real potential in many applications including catalysis, [24–26] bioinorganic modelling [27,28] and molecule magnetism [29–31] and in

the design of molecular machines [32]. More recently, ambidentate ligands have been successfully utilized with metal ions such as Pd(II), Pt(II) and Cu(I) to provide a series of metallosupramolecular complexes with different levels of dynamicity and high catalytic activity in important processes such as the Suzuki–Miyaura, alkene hydrosilylation and Ullmann reactions [24–26].

The isomeric ligands L1, L2 and L3 (Figure 1) have a number of possible coordination modes, even on a single metal centre. As neutral species, all could act as *O,O*-chelates through the β-diketone unit (in either its true diketone or keto-enol form) or as simple *N*-donors through the pyridine ring, with only L3 having the additional possibility of acting as an *N,O*-chelate. As neutral but zwitterionic species resulting from proton transfer from O to N, all three could act exclusively as *O,O*-chelates. In their anionic forms resulting from deprotonation of the β-diketone unit, the same possibilities arise as that for the neutral ligand, although it would be anticipated that the negatively charged diketonate site would now be much more strongly favoured over the neutral *N*-site. In no case is it possible for all donor atoms to be bound to one metal ion so that such ligands must have the capacity to act as bridging species in coordination polymers and metal-organic frameworks, the dimensionality of such species being determined by the stereochemistry of the metal ion involved. Thus, L1–L3 together with an appropriately selected metal ion were expected to be suitable for the synthesis of topologically distinct low-dimensional (1D and 2D) coordination frameworks. Indeed, bridging by the anionic form of ligands related to L1 and L2 by replacement of the *tert-butyl* group by methyl or phenyl has been observed in their Cu(II) coordination polymers [33,34]. In addition, other supramolecular interactions encoded in the structure of the ligands were expected to play an important role in determining and stabilizing such types of extended metal-ion assemblies. Despite the fact that low-dimensional coordination assemblies present more flexible frameworks than 3D polymers, little attention has so far been paid to, e.g., the adsorption properties of this type of metal-organic systems. Thus, by combination of Cu(II) metal centres with the three isomeric pyridyl-β-diketonates ligands L1–L3, we anticipated that the metallosupramolecular assemblies obtained (N1–N2 and C1) would differ not only with respect to their structure and topology but also, as a result of that, in physicochemical properties as well. The present work describes our efforts to explore this hypothesis.
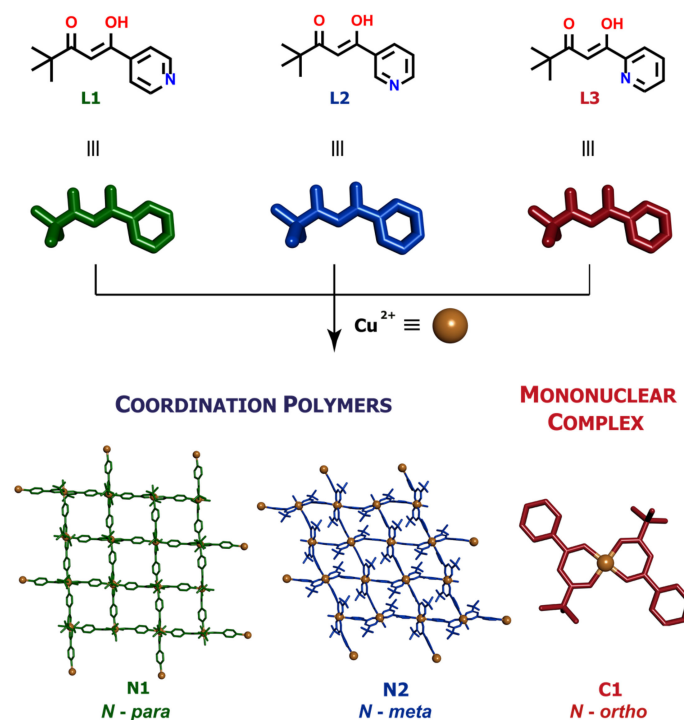

Figure 1. Synthetic routes for the Cu(II) metallosupramolecular architectures based on the pyridyl-β-diketonate ligands.

2. Results and Discussion

2.1. Synthesis and Analysis

The ligands were prepared by Claisen condensation, following a modified literature procedure and involving the reaction between the methyl esters of isonicotinic (for L1), nicotinic (for L2) or picolinic (for L3) acids and pinacolone in the presence of a strong base [24,35]. Depending on the position of the nitrogen atom in the pyridine ring, structurally distinct assemblies were obtained: two coordination polymers N1 (*para-N*) and N2 (*meta-N*) and a monomeric complex C1 (*ortho-N*). All complexes were obtained by the reaction between the appropriate ligand and Cu(II) salt in 2:1 ratio. Although the reported complexes are neutral species, the reactant counterion was of great importance. The best yields were obtained when acetate or nitrate were employed. With other salts such as halides or sulphates, highly insoluble material immediately precipitated from the reaction mixture, preventing further analysis. Optimal procedures with different ligands varied slightly. Best yields in C1 synthesis were obtained when copper acetate was reacted with L3 at room temperature in THF/MeOH (tetrahydrofuran/methanol) (1:1, *v/v*). That procedure proved to be inefficient in preparing N1 and N2, where better yields were obtained when the reaction was carried out in the presence of a stronger base (Na_2CO_3) and at a slightly elevated temperature (40 °C). In each case, green crystals were formed by slow evaporation of the reaction mixture. Crystallization of polymers N1 and N2 took a long time (around 6 weeks), giving crystals of good quality. The solid complexes were characterized by elemental analysis, single crystal X-ray diffraction and XRD powder diffraction. High-resolution ESI-MS spectrometry also demonstrated the presence of the expected fragmentary constituents of each (Figure 2, Figures S4, S7 and S10).
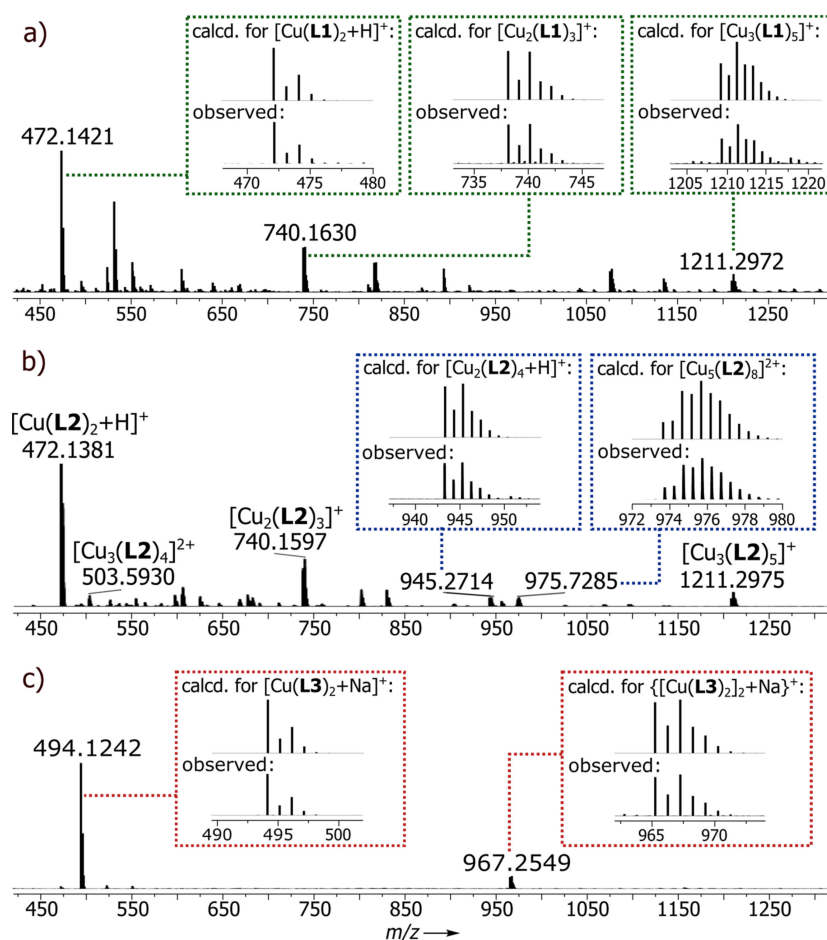

Figure 2. ESI-Q-TOF-HRMS spectra of Cu(II) metal-organic assemblies (**a**) N1, (**b**) N2 and (**c**) C1.

2.2. X-ray Structure Determinations

2.2.1. Ligand [HL3][NO$_3$]

During one attempted preparation of complex C1, crystals of the uncoordinated ligand L3 in the form of nitrate salt were obtained. The crystal structure established protonation of the pyridine nitrogen atom and H-bonding interactions between methine, two aromatic protons and the nitrate counterion (Figure 3a). The protonated ligand in its crystal adopts its enol form similarly to the previously described neutral version of L2 (Figure 3b) [24]. This tautomer is stabilized by a strong resonance-assisted intramolecular hydrogen bond [36] involving O1-H···O2 (1.618 Å).
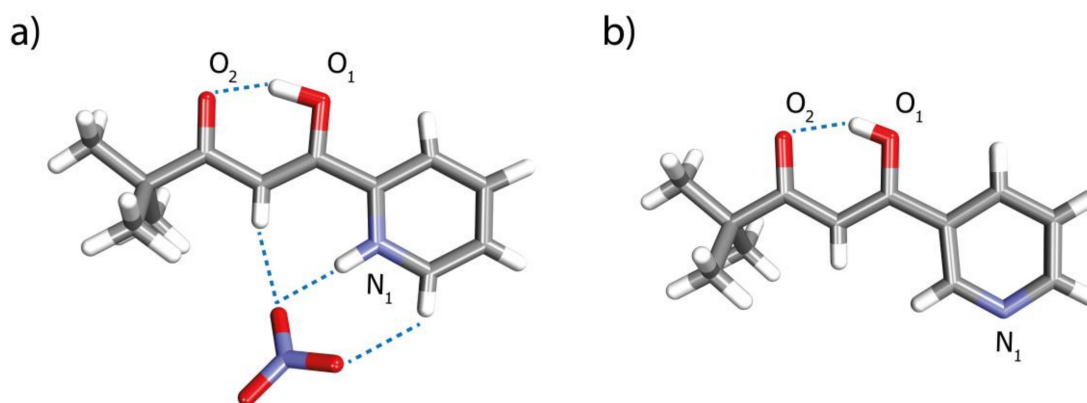

Figure 3. X-ray structures of (**a**) ionic L3 and (**b**) neutral L2 reported previously [24].

2.2.2. Network N1

The structure of [Cu(L1)$_2$]$_n$ in solid state was established by a single crystal X-ray determination as being built up from sheets of a two-dimensional rhombic grid-like coordination polymer lying parallel to the (101) crystallographic plane, analogous to previously reported examples [33,34]. All Cu atoms are equivalent, and each is six coordinates with distorted octahedral geometry (*C2$_h$* local symmetry), being bound within an O$_4$ plane from two *trans*-oriented β-diketonate groups (Cu–O 1.954(1) and 1.958(1) Å) with two axially located nitrogen atoms from pyridyl groups (Cu–N 2.396(1) Å, Figure 4a). Each almost square, grid-like Cu$_4$ unit, edge length Cu···Cu 9.271 Å, defines with its ligands a rhomboidal cavity with dimensions of 9.286 × 9.553 Å and a calculated interior volume of 180 Å^3 (Figure 4b,c and Figure S13). This cavity contains no solvent molecules, as confirmed by thermogravimetric (TGA) analysis (see below). The *trans* arrangement of the two diketonate ligands on Cu means that the *tert-butyl* substituents at each Cu centre lie above and below the mean plane of the polymer, thus producing a lipophilic face on each side of the sheet.

Packing of the sheets of polymers is such that the cavities in each layer are capped by the *tert*-butyl groups projecting from adjacent layers (Figure 5). This leads to dispersion interactions between the methyl groups and the pyridine units forming the wall of the cavity. These intermolecular weak forces may produce flexible parts in the porous network so that the system can exhibit certain dynamicity in the solid state, depending on the external perturbations. The layer-to-layer self-inclusion may somewhat hinder access of the guest molecules inside the pores of the N1 structure but does not exclude application of complexes with such characteristics in gas sorption [37].
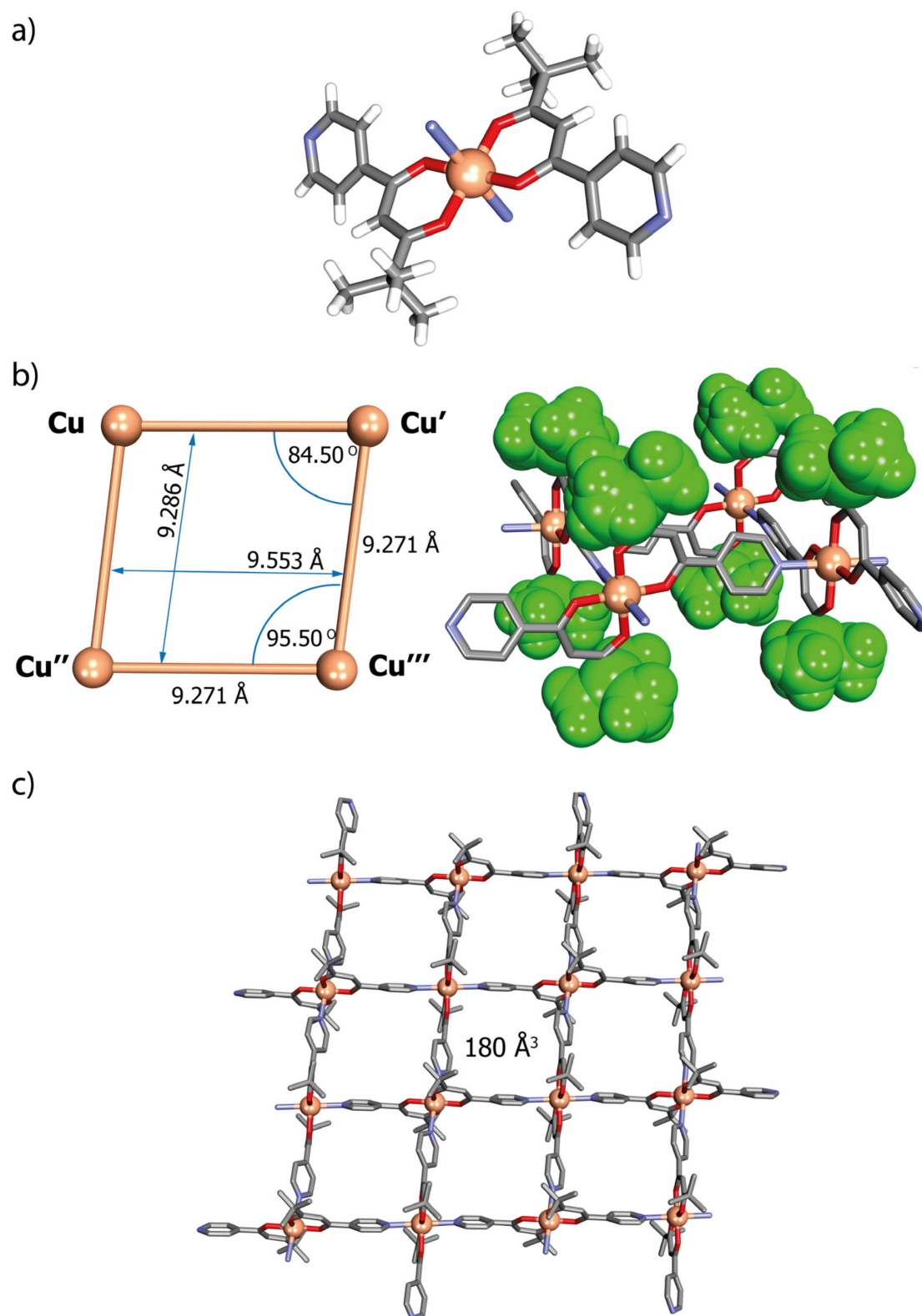
a)

b)

c)

Figure 4. The crystal structure of $[Cu(L1)_2]_n$ (N1) showing (**a**) one of the $[Cu(L1)_2]$ units coordinated to two pyridine nitrogen atoms from neighbouring metalloligands; (**b**) one of the Cu_4 rhombic-grid units with cavity dimensions; and (**c**) the two-dimensional single sheet structure adopted by N1 parallel to the (101) crystallographic plane: H-atoms have been omitted for clarity.
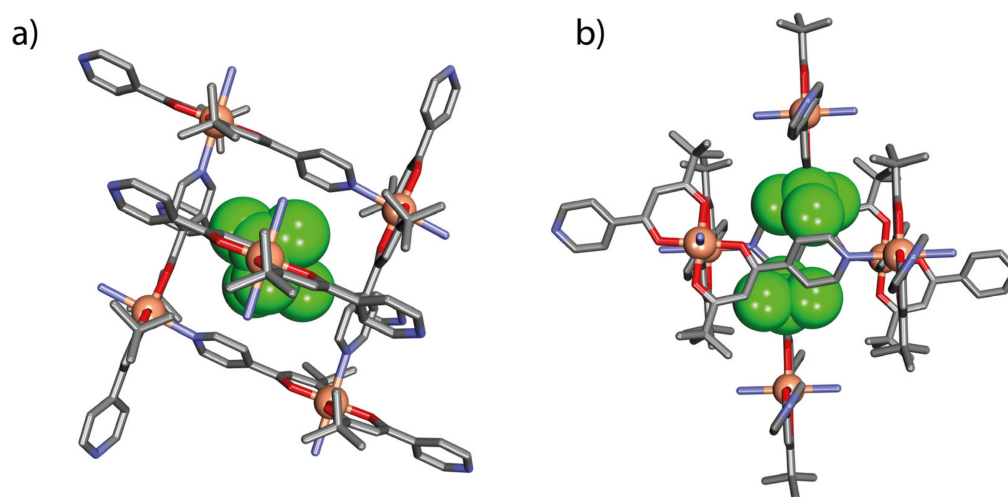
Figure 5. Self-inclusion between adjacent coordination layers of C1: (**a**) top view parallel to the (101) crystallographic plane and (**b**) side view parallel to the (5-4-3) crystallographic plane. H-atoms have been omitted for clarity.

2.2.3. Network N2

Crystals of the polymer $[Cu(L2)_2]_n$ suitable for crystallographic measurements were obtained by slow evaporation of a THF solution. The polymer crystallizes as shiny green rhombic blocks in the monoclinic space group $P2_1/n$. As in N1, all Cu atoms are equivalent and have, as a result again of binding to both diketonate and pyridine donors, the same $C2_h$-symmetric *trans*-N_2O_4 coordination geometry, with very similar bond lengths (Cu-O, 1.949(1) and 1.955(1) Å; Cu-N, 2.409(2) Å). The change in position of the nitrogen donor atom from *para* (N1) to *meta* (N2), although not affecting the coordination mode around the central atom, causes several significant changes in the structure. Although a 2D polymer forming sheets parallel, here, to (10-1) is again present, the Cu_4 units which can be regarded as having been fused to form the polymeric sheet are much further from square (Figure 6), with a shorter side length (8.40(1) Å), and the sheet itself is much more compact. Thus, the rhomboidal cavity of the Cu_4 unit is both strongly tilted and smaller (6.600 × 8.573 Å), and in contrast to N1, the *tert*-butyl groups are directed into the cavity, with the external faces of the sheet being made up of both aliphatic and aromatic (pyridine) CH units. Despite similarity to a system reported by Domasevitch, [33] entirely different packing is observed in the case of the system described by Gloe and Lindoy, showing disordered structure, in which two types of five-coordinated Cu(II) occur [34].

2.2.4. Complex C1

While *N,O* chelation would seem to be a possible mode of coordination for L3, it is clearly not favoured over *O,O* chelation (of the diketonate form), an interaction which appears to inhibit any *N*-coordination and thus polymerization, as shown by the presence of molecular bis(diketonate) species in the crystal structures of the isolated complex. In contrast to the previously reported Cu complex with phenyl substituted linker, [34] C1 crystallizes in two distinct polymorphic forms, triclinic P-1 (tC1) and monoclinic $P2_1/n$ (mC1), in both of which the complex has a distorted square planar geometry around the copper centre with two anionic *O,O'*-chelates from β-diketonate moieties coordinated in a *trans* planar fashion (Figure 7a) [38] There are only very minor differences between the polymorphs (Figure 7b). The Cu–O distances are 1.904–1.907 Å and 1.914–1.917 Å for tC1 and mC1, respectively. In both polymorphs, the diketonate and attached pyridine units are close to coplanar, indicating a significant degree of conjugation. In the monoclinic form, the slipped stacks of complex units which lie in columns parallel to the *b* axis (Figure 7) are linked by weak CH⋯N interactions involving the pyridine-*N* and its adjacent CH, while in the triclinic form, these interactions, now between columns lying parallel to *a*, appear to be much weaker. In both slipped stacks, the interplanar distances

are quite short (3.370 Å for tC1 and 3.217 Å for mC1), indicating significant dispersion interactions. The noncovalent ligation in the apical position in C1 may impose some degree of flexibility in the crystal lattice [39].

2.3. Powder X-ray Diffraction (PXRD) Analyses

The phase purities of as-synthesized samples of coordination compounds N1–N2 and C1 in solid state (Figure 8) were characterized by Powder X-ray Diffraction (PXRD) at 25 °C. The experimental PXRD patterns correspond well with those simulated from the single-crystal data, indicating the bulk samples to be a single phase. The as-synthesized C1 PXRD pattern is well-indexed to the calculation of the triclinic phase. In addition, the PXRD profiles indicate that the solids retain their crystallinity on being crushed. The minor difference in reflection intensities observed between the simulated and experimental patterns may be attributed to variation in the preferred orientation of the powder samples during collection of the experimental PXRD data.
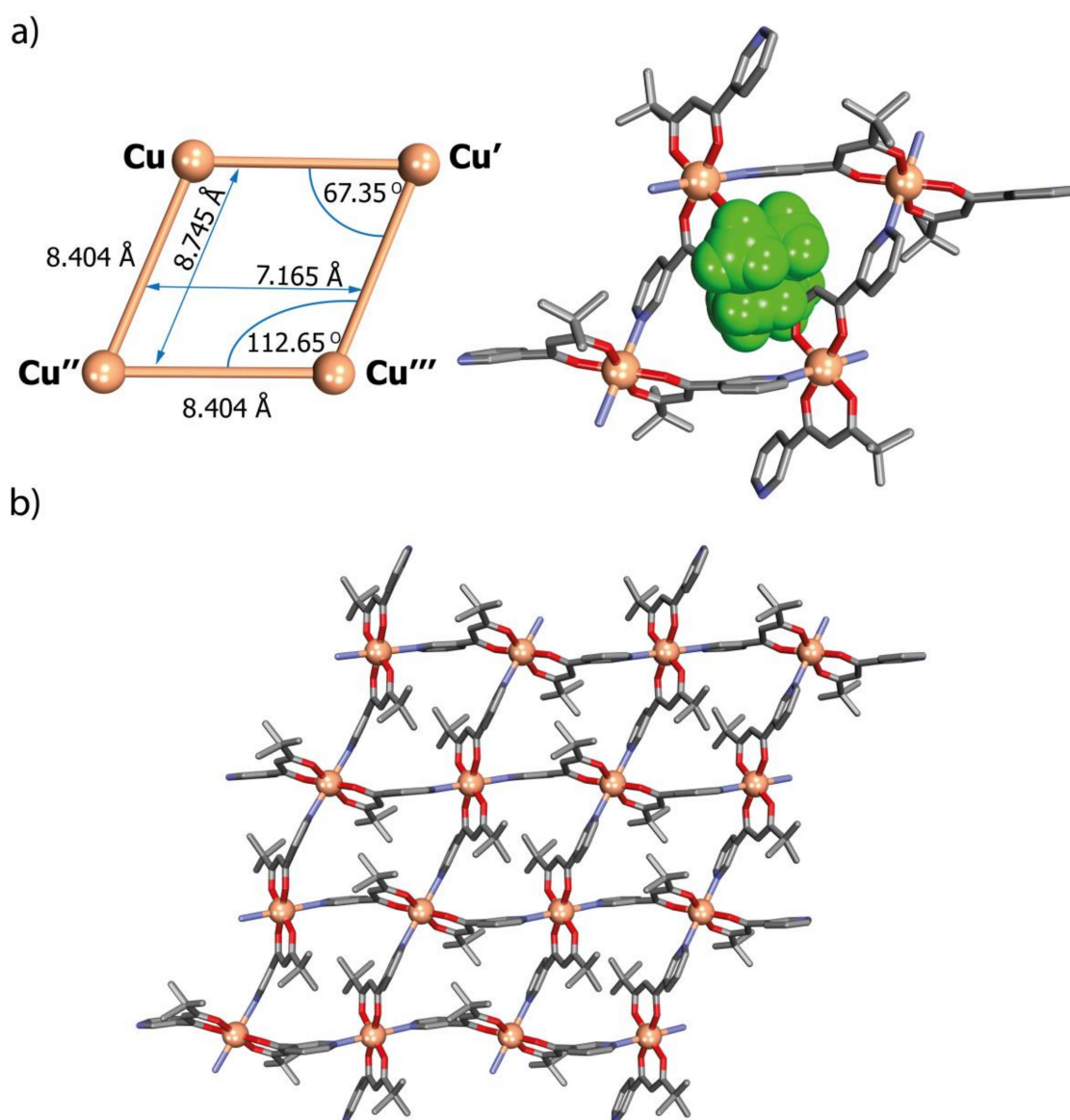

Figure 6. (**a**) Aspects of the geometry of Cu_4 rhombic-grid units (left) with a view of the cavity occupied by the *tert*-butyl groups (right) and (**b**) view of the 2D network of network N2 parallel to the (10-1) crystallographic plane: H-atoms have been omitted for clarity. Disorder of the *tert*-butyl groups is not shown.
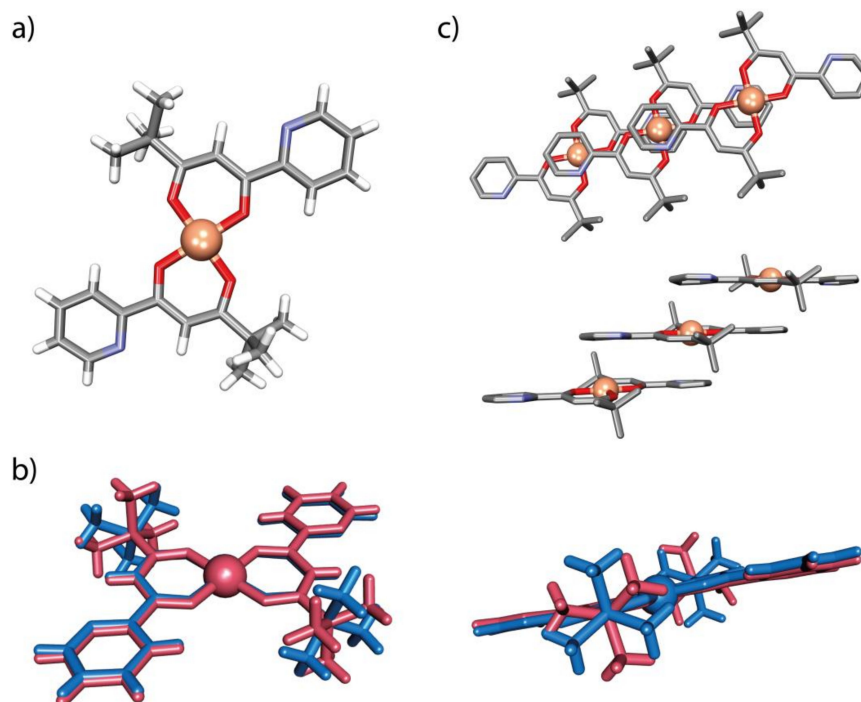
Figure 7. (**a**) The molecular species within the crystal structure of Cu(L3)$_2$ (tC1); (**b**) superposition of the molecules of tC1 (red) and mC1 (blue); and (**c**) part of the 1D stacks (top parallel to the (-3-1-2) crystallographic plane and side views parallel to the (-12-1) crystallographic plane) of parallel molecules found in tC1: H-atoms have been omitted for clarity.
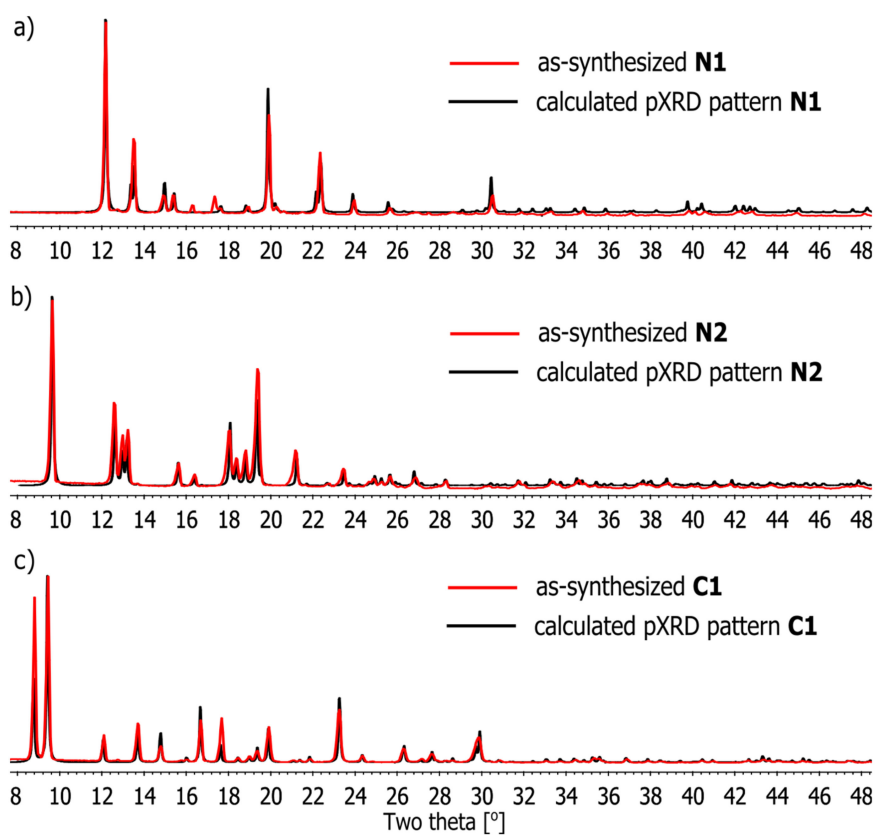

Figure 8. Comparison of powder X-ray diffraction patterns of compounds (**a**) N1, (**b**) N2 and (**c**) C1, as-synthesized (red) and calculated (black) from single-crystal X-ray data of N1–N2 and C1.

2.4. SEM Analysis

The solid coordination polymers (N1 and N2) were investigated by scanning electron microscopy (SEM) to get visual insights into their morphologies. The images were recorded with an accelerating voltage of 20 kV and magnification up to ×30,000 using an LFD (large field detector) in solid state. Initially, the powdered samples of the appropriate complex were applied to a Si/SiO_2 substrate and dried under vacuum. The morphologies of coordination polymers N1 and N2 were found to be quite distinct, though the complexes differ only in the position of the nitrogen atom in the pyridine ring. The SEM images of N1 (Figure 9a and Figure S6) indicate the formation of fibre-shaped morphology, with an estimated average length of up to 20 µm. The fibres intertwine in three dimensions, giving a dense-packed network. The SEM image of N2 exhibits diverse polymeric morphology, with the average length of the fibres decreased by 5 times (approx. 4 µm, Figure 9b and Figure S9). The shrinkage in fibre length of N2 occurs probably due to the formation of a more densely packed coordination network, which is consistent with the data obtained from the X-ray studies. The SEM analysis divulges that the synthesized coordination assemblies remained in polymeric form and confirms the significant impact of the polymers' crystal packing on the morphology of the nanostructure formed. For comparison, SEM images were also recorded for the C1 complex (Figure 9c,d and Figure S12). In contrast to the two previously discussed assemblies, C1 appear as single microcrystals rather than polymeric networks, approx. 20–100 µm with a triclinic crystalline phase.
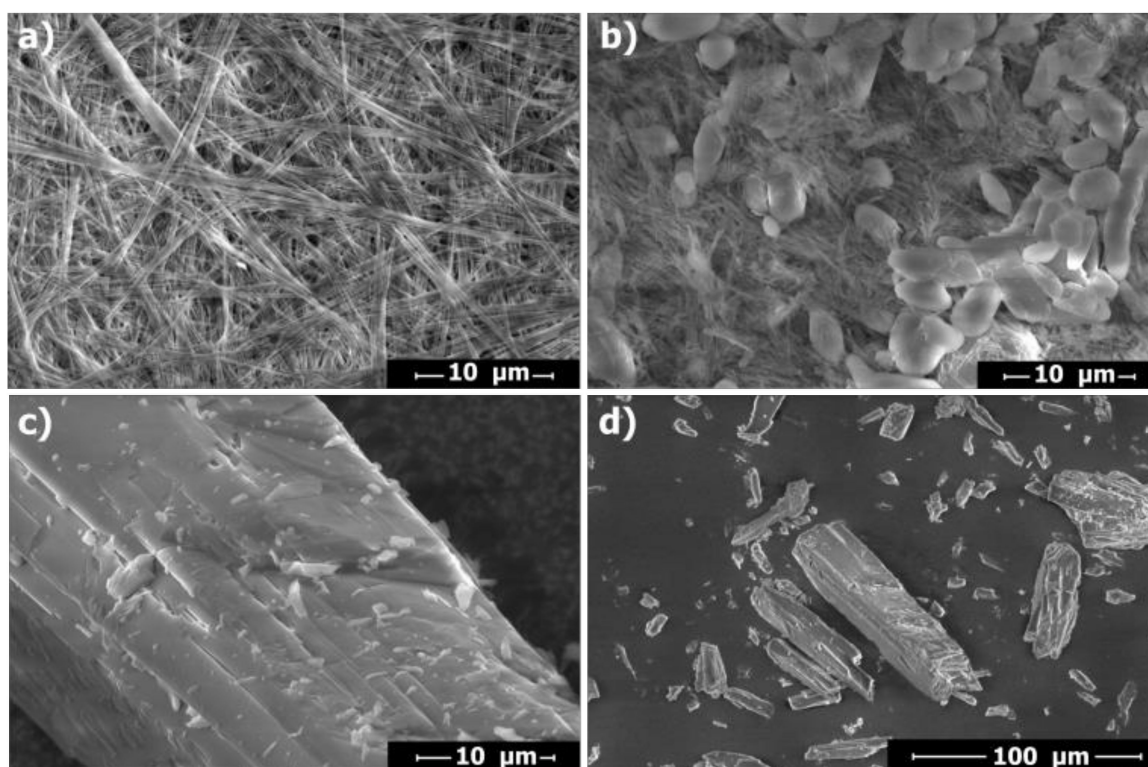

Figure 9. Scanning electron microscopy (SEM) images of complexes (**a**) N1, (**b**) N2 and (**c**,**d**) triclinic form C1.

2.5. Framework Thermal Stability

Thermogravimetric analysis (TGA) was conducted to study the thermal stability of compounds N1–N2 and C1 (Figure 10). The experiments were performed on crystalline samples (approx. 5 mg) in the temperature range 25–650 °C under N_2 atmosphere with a heating rate of 10 °C/min. The TGA curves of polymers N1 and N2 have similar profiles and show high stability of these materials with no weight loss of up to 300 and 250 °C, respectively, after which the framework structure begins to

collapse (Figure 10, Figures S5 and S8, blue and black curves, respectively). Two-stage decomposition via gradual removal of organic components of compounds N1 and N2 occurs from 300 and 250 °C to 420 and 440 °C, respectively, leading to the formation of copper oxides as the residue (Cu_2O for N1 calcd. 30.31% and found 30.02% and CuO for N2 calcd. 16.85% and found 18.90%). The TGA pattern of C1 is slightly different (Figure 10 and Figure S11, red curve), which results from the dimeric nature of this complex compared to polymeric N1 and N2. The crystal plateaus steadily until 230 °C, after which a stepwise decomposition of the organic ligands occurs (from 230 to 590 °C), finally giving predominantly a CuO residue (calcd. 14.62% and found 16.34%).
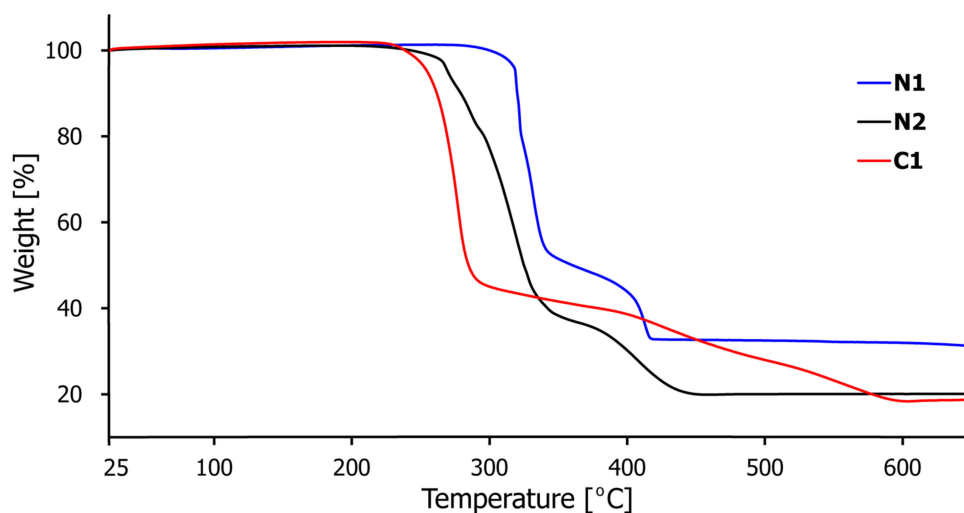

Figure 10. The thermogravimetric analysis (TGA) curves for coordination polymers N1–N2 and complex C1.

2.6. Gas Sorption Studies

CPs have been proposed as promising gas adsorbents due to their high stability and well-defined porous structures. While these materials are intensively focused on frameworks consisting of polydentate linkers, neutral systems based on ambidentate ligands are much less explored [40–44]. This prompts us to evaluate gas sorption properties of N1–N2 and C1 despite relatively low porosity of the complexes as indicated by X-ray analysis (Table S1). The adsorption/desorption isotherms for N_2 were measured for degassed frameworks of N1–N2 and C1 at 77.35 K (Figure S14). All three complexes presented very low sorption values in the pressure range of 0–800 mmHg (Table S2), consistent with the fact that these materials have no obvious pores. The values of Brunauer–Emmett–Teller isotherm (BET) surface areas (1.9–4.3 m^2g^{-1}) obtained for all three complexes confirmed their nonporous nature, and despite their promising 2D topology, potential applications in this area would require considerable structural modifications in the ligand structure.

3. Materials and Methods

3.1. General Methods

All chemicals and solvents were obtained from commercial sources and used as received. THF was dried by distillation with benzophenone/sodium prior to use. The ^{1}H NMR spectra were acquired on a Bruker Fourier 300 spectrometer equipped with a ^{1}H 5 mm probe and referenced to the solvent residual peaks. All spectra were acquired at 24.85 °C. NMR solvents were purchased from Deutero GmbH (Kastellaun, Germany) and used as received. ESI-MS spectra were recorded on a Bruker Impact HD Q-TOF spectrometer in the positive ion mode. Thermogravimetric analysis (TGA) was performed using a STA4000 (Perkin Elmer–Waltham, MA, USA) instrument between 25 and 650 °C in a N_2 atmosphere with a flow rate of 20 mL min^{-1} and a heating rate of 10 °C min^{-1}. Powder X-ray diffraction

patterns (PXRD) were recorded on a BRUKER D8-Focus Bragg-Brentano X-ray powder diffractometer equipped with a Cu sealed tube (λ = 1.54178Å) at room temperature. The scans were collected in the 2θ range of 5–50°. Experimental and calculated powder patterns from the crystal structures were analysed using Kdif software. A zero point correction was applied to the experimental data for N1 (−0.05), N2 (−0.12) and C1 (0.05). The morphologies of the solid complexes were characterized by scanning electron microscopy (SEM, XL 30 ESEMFEG FEI Company–Hillsboro, ORE, USA). The void volume was visualized and calculated using Digital Discovery Studio 3.5. Brunauer–Emmett–Teller (BET) surface areas were determined by N_2 adsorption at −196 °C. Prior to the measurements of adsorption/desorption isotherms, the samples were outgassed for 20 h under a pressure of 0.25 mm Hg. Elemental analyses were performed on the apparatus of the German company an Elementar (Langenselbold, Germany), model Vario EL III.

3.2. X-ray Crystallography

X-ray structure determinations for N2, tC1 and [HL3][NO$_3$] were performed on a 4-circle Xcalibur EosS2 diffractometer (Agilent Technologies) equipped with a CCD (Charge-coupled Device) detector. X-ray data were collected at room temperature using graphite-monochromated MoKα radiation (λ = 0.71073 Å) with the ω-scan technique. The crystal tC1 used for the measurements was identified as a non-merohedral twin with the twin matrix (-1 0 0 0 -1 0 0.997 0.271 1) corresponding to 180° rotation about the (001) reciprocal lattice direction. Olex2 [45] was used as an interface for structure solution, refinement and structural analysis. The crystal structure of tC1 was solved using ShelXT-2015 [46] and was refined with SHELXL-2015 [47] using the diffraction intensity data written in HKLF 5 format.

The X-ray diffraction data for N1 and mC1 were collected on an Oxford Diffraction SuperNova diffractometer equipped with a CuKα radiation source (λ = 1.54178 Å) and with a Cryojet cooling system. For data reduction, UB-matrix determination and absorption correction, CrysAlisPro [48] and CrysAlisRed [49] software were applied. Using Olex2 [45], the structures were solved with intrinsic phasing methods employing ShelXT-2015 [46] and were refined by full-matrix least-squares against F^2 with the help of the SHELXL-2015 [47] refinement package using least squares minimization. All non-hydrogen atoms were refined anisotropically. Some of the hydrogen atoms were derived from a difference Fourier map, and they were refined isotropically. The remaining H-atoms were located in idealized positions by molecular geometry and were refined as riding groups with U_{iso} (H) = *1.2 U_{eq}(C)* or *1.5 U_{eq}(O)*. Selected structural parameters are reported in Table 1. The data have been deposited in the Cambridge Crystallographic Data Collection (CCDC), deposition numbers CCDC 1979395-1979398 and 2009855. These data can be obtained free of charge via www.ccdc.cam.ac.uk/data_request/cif, by emailing data_request@ccdc.cam.ac.uk, or by contacting The Cambridge Crystallographic Data Centre, 12, Union Road, Cambridge CB2.

Table 1. Crystal data and structure refinement for coordination compounds N1–N2 and C1 and for ligand [HL3][NO3].

Parameters	N1–[Cu(L1)2]n	N2–[Cu(L2)2]n	tC1–Cu(L3)2	mC1–Cu(L3)2	[HL3][NO3]
CCDC code	1979395	1979396	2009855	1979398	1979397
Empirical formula	$C_{24}H_{28}CuN_2O_4$	$C_{24}H_{28}CuN_2O_4$	$C_{24}H_{28}CuN_2O_4$	$C_{24}H_{28}CuN_2O_4$	$C_{12}H_{16}N_2O_5$
Formula weight	472.02	472.02	472.02	472.02	268.27
Temperature/K	130.6(3)	293(2)	293(2)	133(2)	293(2)
Crystal system	monoclinic	monoclinic	triclinic	Monoclinic	Monoclinic
Space group	$P2_1/n$	$P2_1/n$	P-1	$P2_1/n$	$P2_1/c$
a/Å	9.67360(10)	11.5058(3)	6.3111(8)	13.1273(6)	11.3313(4)
b/Å	12.46690(10)	9.3195(2)	9.4952(11)	6.0457(2)	10.0225(4)
c/Å	9.73330(10)	12.3363(3)	10.5041(13)	14.2591(5)	11.9033(5)
α/°	90	90	94.356(10)	90	90
β/°	90.0270(10)	108.256(3)	106.293(11)	92.322(3)	91.277(3)
γ/°	90	90	98.971(10)	90	90
Volume/Å³	1173.83(2)	1256.22(6)	592.01(13)	1130.73(8)	1351.50(9)
Z	2	2	1	2	4
ρ_{calc}g/cm³	1.335	1.248	1.324	1.386	1.318
μ/mm⁻¹	1.569	0.898	0.953	1.629	0.103
F(000)	494.0	494.0	247.0	494.0	568.0
Crystal size/mm³	0.62 × 0.36 × 0.34	0.15 × 0.1 × 0.05	0.3 × 0.05 × 0.03	0.2 × 0.1 × 0.02	0.2 × 0.15 × 0.1
Radiation	Cu Kα (λ = 1.54184)	MoKα (λ = 0.71073)	MoKα (λ = 0.71073)	CuKα (λ = 1.54184)	MoKα (λ = 0.71073)
2Θ range for data collection/°	11.578 to 152.524	8.218 to 53.446	8.528 to 50.042	8.978 to 152.556	6.46 to 59.074
Index ranges	−10 ≤ h ≤ 12, −15 ≤ k ≤ 15, −12 ≤ l ≤ 10	−14 ≤ h ≤ 14, −11 ≤ k ≤ 11, −15 ≤ l ≤ 15	−7 ≤ h ≤ 7, −11 ≤ k ≤ 11, −6 ≤ l ≤ 12	−15 ≤ h ≤ 16, −7 ≤ k ≤ 7, −17 ≤ l ≤ 12	−15 ≤ h ≤ 15, −13 ≤ k ≤ 13, −14 ≤ l ≤ 14
Reflections collected	21,676	56,535	2094	4407	50,829
Independent reflections	2428 (Rint = 0.0320, Rsigma = 0.0123)	2662 (Rint = 0.0444, Rsigma = 0.0160)	2094 (Rint = merged, Rsigma = 0.0956)	2299 (Rint = 0.0209, Rsigma = 0.0254)	3209 (Rint = 0.0762, Rsigma = 0.0317)
Data/restraints/parameters	2428/0/188	2662/0/166	2094/0/146	2299/0/176	3209/0/214
Goodness-of-fit on F²	1.083	1.038	1.096	1.074	1.098
Final R indexes [I ≥ 2σ (I)]	R1 = 0.0321, wR2 = 0.0860	R1 = 0.0359, wR2 = 0.0928	R1 = 0.0701, wR2 = 0.1488	R1 = 0.0460, wR2 = 0.1288	R1 = 0.0752, wR2 = 0.1715
Final R indexes (all data)	R1 = 0.0325, wR2 = 0.0862	R1 = 0.0448, wR2 = 0.0976	R1 = 0.1134, wR2 = 0.1698	R1 = 0.0517, wR2 = 0.1357	R1 = 0.1101, wR2 = 0.1906
Largest diff. peak/hole/e Å⁻³	0.32/-0.38	0.37/-0.29	0.37/-0.49	0.92/-0.55	0.61/-0.17

3.3. General Preparation of L–L3

The syntheses of 4,4-dimethyl-1-(pyridin-4-yl)-pentane-1,3-dione (L1), 4,4-dimethyl-1-(pyridin-3-yl)-pentane-1,3-dione (L2) and 4,4-dimethyl-1-(pyridin-2-yl)-pentane-1,3-dione (L3) were performed following previously described procedures involving Claisen condensation between appropriate pyridinecarboxylic acid methyl esters and pinacolone in the presence of strong base (NaH) (Figures S1–S3) [24,35].

3.4. Synthesis of [Cu(L1 or 2)2]n–N1 and N2

Ligands L1 or L2 (50 mg, 0.24 mmol) in dry THF (5 mL) were added to Na2CO3 (0.5 g, approximately 5 mmol) suspended in dry THF (10 mL). The mixture was stirred for 1 h before Cu(NO3)2·5H2O (34 mg, 0.12 mmol) (alternatively Cu(CH3CO2)2·H2O (24 mg, 0.12 mmol)) in dry THF (5 mL) was added dropwise. The resulting mixture was stirred at 40 °C for 2 h. The excess Na2CO3 was filtered off, and slow evaporation of the filtrate gave greenish crystals which were collected and washed with EtOH and Et2O. Yields were 74% and 71% for N1 and N2, respectively. The coordination polymers N1 and N2 can also be obtained in the form of powders through precipitation with *n*-hexane from the reaction mixture, previously concentrated under reduced pressure. The XRD powder patterns are in full agreement with data obtained from X-ray crystallographic analysis.

N1: ESI-Q-TOF-HRMS: calcd. for $C_{24}H_{29}N_2O_4Cu$ [Cu(L1)2+H]⁺: *m/z* = 472.1418, observed: *m/z* = 472.1421; calcd. for $C_{36}H_{42}N_3O_6Cu_2$ [Cu2(L1)3]⁺: *m/z* = 740.1650, observed: *m/z* = 740.1630; calcd. for $C_{38}H_{48}N_3O_7SCu_2$ [Cu2(L1)3+DMSO]⁺: *m/z* = 818.1789, observed: *m/z* = 818.1767; calcd.

for $C_{60}H_{70}N_5O_{10}Cu_3$ $[Cu_3(L1)_5]^+$: m/z = 1211.3000, observed: m/z = 1211.2972; Elem. Anal.: calcd. for $C_{24}H_{28}N_2O_4Cu$: C, 61.07; H, 5.98; N, 5.93. Found: C, 59.81; H, 5.79; N, 5.68 (%).

N2: ESI-Q-TOF-HRMS: calcd. for $C_{24}H_{29}N_2O_4Cu$ $[Cu(L2)_2+H]^+$: m/z = 472.1418, observed: m/z = 472.1381; calcd. for $C_{48}H_{56}N_4O_8Cu_3$ $[Cu_3(L2)_4]^{2+}$: m/z = 503.5983, observed: m/z = 503.5930; calcd. for $C_{36}H_{42}N_3O_6Cu_2$ $[Cu_2(L2)_3]^+$: m/z = 738.1660, observed: m/z = 738.1687; calcd. for $C_{72}H_{84}N_6O_{12}Cu_4$ $[Cu_4(L2)_6]^{2+}$: m/z = 739.1658, observed: m/z = 739.1658; calcd. for $C_{48}H_{57}N_4O_8Cu_2$ $[Cu_2(L2)_4+H]^+$: m/z = 945.2757, observed: m/z = 945.2758; calcd. for $C_{96}H_{112}N_8O_{16}Cu_5$ $[Cu_5(L2)_8]^{2+}$: m/z = 975.7333, observed: m/z = 975.7285; calcd. for $C_{60}H_{70}N_5O_{10}Cu_3$ $[Cu_3(L2)_5]^+$: m/z = 1211.3000, observed: m/z = 1211.2975; Elem. Anal.: calcd. for $C_{24}H_{28}N_2O_4Cu$: C, 61.07; H, 5.98; N, 5.93. Found: C, 60.95; H, 5.84; N, 5.82 (%).

3.5. Synthesis of Cu(L3)₂–C1

A solution of L3 (50 mg, 0.24 mmol) and $Cu(CH_3COO)_2 \cdot H_2O$ (24 mg, 0.12 mmol) in THF/MeOH (1:1, *v/v*, 10 mL) was stirred at room temperature for 24 h, after which DMSO (1 mL) was added. The mixture was left in air for 7 days at room temperature. Dark green crystals tC1 of the triclinic form slowly deposited. The product was filtered off and washed with EtOH and Et₂O. Single crystals of mC1 as a monoclinic form were obtained by diffusion of *tert*-butyl methyl ether vapours into a THF solution of the complex. Yield was 85%. ESI-Q-TOF-HRMS: calcd. for $C_{24}H_{28}N_2O_4CuNa$ $[Cu(L3)_2+Na]^+$: m/z = 494.1237, observed: m/z = 494.1242; calcd. for $C_{48}H_{56}N_4O_8Cu_2Na$ $\{[Cu(L3)_2]_2+Na\}^+$: m/z = 967.2577, observed: m/z = 967.2549; Elem. Anal.: calcd. for $C_{24}H_{28}N_2O_4Cu$: C, 61.07; H, 5.98; N, 5.93. Found: C, 60.86; H, 5.79; N, 5.78 (%).

4. Conclusions

In summary, we have successfully generated and fully analysed three structurally distinct metallosupramolecular frameworks employing Cu(II) ions and ambidentate pyridyl-β-diketonate ligands. The structural features, stability and morphology of these coordination compounds were determined by single-crystal and powder XRD, TGA, TOF-MS, SEM and elemental analysis. This work demonstrates that variations of the *N*-atom position in the pyridyl ring are critical to the type of metal-organic assembly generated. In addition to significant differences in topology and dimensionality, disparities in physical properties between studied metal-organic assemblies were observed, confirming the determining role of the *N*-atom position not only on the structure but also on the potential function of these materials.

Conflicts of Interest: The authors declare no conflict of interest. The funders had no role in the design of the study; in the collection, analyses or interpretation of data; in the writing of the manuscript; or in the decision to publish the results.

Abbreviations

calcd.	calculated
CCD	Charge-coupled Device
XRD	X-Ray diffraction
PXRD	powder X-Ray diffraction
TGA	thermogravimetric analysis
TOF-MS	time-of-flight mass spectrometry
SEM	scanning electron microscopy
LFD	large field detector
THF	tetrahydrofuran
MeOH	methanol
NaH	sodium hydride
BET	Brunauer–Emmett–Teller isotherm
CPs	coordination polymers

References

1. Gorczyński, A.; Harrowfield, J.M.; Patroniak, V.; Stefankiewicz, A.R. Quaterpyridines as Scaffolds for Functional Metallosupramolecular Materials. *Chem. Rev.* **2016**, *116*, 14620–14674. [CrossRef]
2. Northrop, B.H.; Yang, H.-B.; Stang, P.J. Coordination-driven self-assembly of functionalized supramolecular metallacycles. *Chem. Commun.* **2008**, 5896–5908. [CrossRef] [PubMed]
3. Bocian, A.; Drożdż, W.; Szymańska, M.; Lewandowski, J.; Fik-Jaskółka, M.; Gorczyński, A.; Patroniak, V.; Stefankiewicz, A.R. Complex-decorated surfactant-encapsulated clusters (CD-SECs) as novel multidynamic hybrid materials. *Nanoscale* **2020**, *12*, 4743–4750. [CrossRef]
4. Markiewicz, G.; Walczak, A.; Perlitius, F.; Piasecka, M.; Harrowfield, J.M.; Stefankiewicz, A.R. Photoswitchable transition metal complexes with azobenzene-functionalized imine-based ligands: Structural and kinetic analysis. *Dalton Trans.* **2018**, *47*, 14254–14262. [CrossRef] [PubMed]
5. Drożdż, W.; Walczak, A.; Bessin, Y.; Gervais, V.; Cao, X.-Y.; Lehn, J.-M.; Ulrich, S.; Stefankiewicz, A.R. Multivalent Metallosupramolecular Assemblies as Effective DNA Binding Agents. *Chem. Eur. J.* **2018**, *24*, 10802–10811. [CrossRef] [PubMed]
6. Brzechwa-Chodzyńska, A.; Zieliński, M.; Gilski, M.; Harrowfield, J.M.; Stefankiewicz, A.R. Dynamer and Metallodynamer Interconversion: An Alternative View to Metal Ion Complexation. *Inorg. Chem.* **2020**, *59*, 8552–8561. [CrossRef] [PubMed]
7. Kitagawa, S.; Kitaura, R.; Noro, S.-I. Functional Porous Coordination Polymers. *Angew. Chem. Int. Ed.* **2004**, *43*, 2334–2375. [CrossRef] [PubMed]
8. Janiak, C. Engineering coordination polymers towards applications. *Dalton Trans.* **2003**, 2781–2804. [CrossRef]
9. Duan, J.; Jin, W.; Kitagawa, S. Water-resistant porous coordination polymers for gas separation. *Coord. Chem. Rev.* **2017**, *332*, 48–74. [CrossRef]
10. Uemura, T.; Yanai, N.; Kitagawa, S. Polymerization reactions in porous coordination polymers. *Chem. Soc. Rev.* **2009**, *38*, 1228–1236. [CrossRef]
11. Agarwal, R.A.; Gupta, N.K. CO_2 sorption behavior of imidazole, benzimidazole and benzoic acid based coordination polymers. *Coord. Chem. Rev.* **2017**, *332*, 100–121. [CrossRef]
12. Toma, H.E.; Rocha, R.C. Linkage Isomerization Reactions. *Croatica Chemica Acta* **2001**, *74*, 499–528.
13. Burmeister, J.L. Linkage isomerism in metal complexes. *Coord. Chem. Rev.* **1968**, *3*, 225–245. [CrossRef]
14. Lee, S.-L.; Hu, F.-L.; Shang, X.-J.; Shi, Y.-X.; Tan, A.L.; Mizera, J.; Clegg, J.K.; Zhang, W.-H.; Young, D.J.; Lang, J.-P. Efficient ring-opening polymerization (ROP) of ε-caprolactone catalysed by isomeric pyridyl β-diketonate iron(III) complexes. *New J. Chem.* **2017**, *41*, 14457–14465. [CrossRef]
15. Wu, H.-B.; Wang, Q.-M. Construction of Heterometallic Cages with Tripodal Metalloligands. *Angew. Chem. Int. Ed.* **2009**, *48*, 7343–7345. [CrossRef]

16. Burrows, A.D.; Mahon, M.F.; Renouf, C.L.; Richardson, C.; Warren, A.J.; Warren, J.E. Dipyridyl β-diketonate complexes and their use as metalloligands in the formation of mixed-metal coordination networks. *Dalton Trans.* **2012**, *41*, 4153–4163. [CrossRef] [PubMed]

17. Hou, G.-G.; Liu, Y.; Liu, Q.-K.; Ma, J.-P.; Dong, Y.-B. NbO lattice MOFs based on octahedral M(II) and ditopic pyridyl substituted diketonate ligands: Structure, encapsulation and guest-driven luminescent property. *Chem. Commun.* **2011**, *47*, 10731–10733. [CrossRef]

18. Liu, F.; Zhou, Y. Polymeric [Eu(L)$_3$(H$_2$O)] (HL = 1-(pyridin-4-yl)butane-1,3-dione and Dimeric [Eu$_2$(L)$_6$(H$_2$O)$_2$] (HL = 1,3-di(pyridin-3-yl)propane-1,3-dione) as selective and sensitive chemosensors for Hg(II) ion. *Inorg. Chem. Commun.* **2010**, *13*, 1410–1413. [CrossRef]

19. Wang, M.; Vajpayee, V.; Shanmugaraju, S.; Zheng, Y.-R.; Zhao, Z.; Kim, H.; Mukherjee, P.S.; Chi, K.-W.; Stang, P.J. Coordination-Driven Self-Assembly of M$_3$L2 Trigonal Cages from Preorganized Metalloligands Incorporating Octahedral Metal Centers and Fluorescent Detection of Nitroaromatics. *Inorg. Chem.* **2011**, *50*, 1506–1512. [CrossRef]

20. Carlucci, L.; Ciani, G.; Proserpio, D.M.; Visconti, M. The novel metalloligand [Fe(bppd)$_3$] (bppd = 1,3-bis(4-pyridyl)-1,3-propanedionate) for the crystal engineering of heterometallic coordination networks with different silver salts. Anionic control of the structures. *CrystEngComm* **2011**, *13*, 5891–5902. [CrossRef]

21. Zhang, Y.; Chen, B.; Fronczek, F.R.; Maverick, A.W. A Nanoporous Ag−Fe Mixed-Metal−Organic Framework Exhibiting Single-Crystal-to-Single-Crystal Transformations upon Guest Exchange. *Inorg. Chem.* **2008**, *47*, 4433–4435. [CrossRef] [PubMed]

22. Andrews, P.C.; Deacon, G.B.; Frank, R.; Fraser, B.H.; Junk, P.C.; MacLellan, J.G.; Massi, M.; Moubaraki, B.; Murray, K.S.; Silberstein, M. Formation of Ho[III] Trinuclear Clusters and Gd[III] Monodimensional Polymers Induced by *ortho* and *para* Regioisomers of Pyridyl-Functionalised β-Diketones: Synthesis, Structure, and Magnetic Properties. *Eur. J. Inorg. Chem.* **2009**, *2009*, 744–751. [CrossRef]

23. Chen, B.; Fronczek, F.R.; Maverick, A.W. Porous Cu−Cd Mixed-Metal−Organic Frameworks Constructed from Cu(Pyac)$_2$ {Bis[3-(4-pyridyl)pentane-2,4-dionato]copper(II)}. *Inorg. Chem.* **2004**, *43*, 8209–8211. [CrossRef] [PubMed]

24. Walczak, A.; Stefankiewicz, A.R. pH-Induced Linkage Isomerism of Pd(II) Complexes: A Pathway to Air- and Water-Stable Suzuki–Miyaura-Reaction Catalysts. *Inorg. Chem.* **2018**, *57*, 471–477. [CrossRef] [PubMed]

25. Walczak, A.; Stachowiak, H.; Kurpik, G.; Kaźmierczak, J.; Hreczycho, G.; Stefankiewicz, A.R. High catalytic activity and selectivity in hydrosilylation of new Pt(II) metallosupramolecular complexes based on ambidentate ligands. *J. Catal.* **2019**, *373*, 139–146. [CrossRef]

26. Abdine, R.A.A.; Kurpik, G.; Walczak, A.; Aeash, S.A.A.; Stefankiewicz, A.R.; Monnier, F.; Taillefer, M. Mild temperature amination of aryl iodides and aryl bromides with aqueous ammonia in the presence of CuBr and pyridyldiketone ligands. *J. Catal.* **2019**, *376*, 119–122. [CrossRef]

27. Lee, J.; Kovalevsky, A.Y.; Novozhilova, I.V.; Bagley, K.A.; Coppens, P.; Richter-Addo, G.B. Single- and Double-Linkage Isomerism in a Six-Coordinate Iron Porphyrin Containing Nitrosyl and Nitro Ligands. *J. Am. Chem. Soc.* **2004**, *126*, 7180–7181. [CrossRef]

28. Van Rijt, S.H.; Hebden, A.J.; Amaresekera, T.; Deeth, R.J.; Clarkson, G.J.; Parsons, S.; McGowan, P.C.; Sadler, P.J. Amide Linkage Isomerism As an Activity Switch for Organometallic Osmium and Ruthenium Anticancer Complexes. *J. Med. Chem.* **2009**, *52*, 7753–7764. [CrossRef]

29. Coronado, E.; Giménez-López, M.C.; Levchenko, G.; Romero, F.M.; García-Baonza, V.; Milner, A.; Paz-Pasternak, M. Pressure-Tuning of Magnetism and Linkage Isomerism in Iron(II) Hexacyanochromate. *J. Am. Chem. Soc.* **2005**, *127*, 4580–4581. [CrossRef]

30. Shatruk, M.; Dragulescu-Andrasi, A.; Chambers, K.E.; Stoian, S.A.; Bominaar, E.L.; Achim, C.; Dunbar, K.R. Properties of Prussian Blue Materials Manifested in Molecular Complexes: Observation of Cyanide Linkage Isomerism and Spin-Crossover Behavior in Pentanuclear Cyanide Clusters. *J. Am. Chem. Soc.* **2007**, *129*, 6104–6116. [CrossRef]

31. Coronado, E.; Giménez-López, M.C.; Korzeniak, T.; Levchenko, G.; Romero, F.M.; Segura, A.; García-Baonza, V.; Cezar, J.C.; de Groot, F.M.F.; Milner, A.; et al. Pressure-Induced Magnetic Switching and Linkage Isomerism in K$_{0.4}$Fe$_4$[Cr(CN)$_6$]$_{2.8}$·16H$_2$O: X-ray Absorption and Magnetic Circular Dichroism Studies. *J. Am. Chem. Soc.* **2008**, *130*, 15519–15532. [CrossRef] [PubMed]

32. Castellano, M.; Ruiz-García, R.; Cano, J.; Ferrando-Soria, J.; Pardo, E.; Fortea-Pérez, F.R.; Stiriba, S.-E.; Barros, W.P.; Stumpf, H.O.; Cañadillas-Delgado, L.; et al. Metallosupramolecular approach toward multifunctional magnetic devices for molecular spintronics. *Coord. Chem. Rev.* **2015**, *303*, 110–138. [CrossRef]

33. Domasevitch, K.V.; Vreshch, V.D.; Lysenko, A.B.; Krautscheid, H. Two-dimensional square-grid frameworks formed by self-associating copper(II) complexes with 1-(3-pyridyl)- and 1-(4-pyridyl)-substituted butane-1,3-diones. *Acta Crystallographica C* **2006**, *62*, m443–m447. [CrossRef] [PubMed]

34. Dudek, M.; Clegg, J.K.; Glasson, C.R.K.; Kelly, N.; Gloe, K.; Gloe, K.; Kelling, A.; Buschmann, H.-J.; Jolliffe, K.A.; Lindoy, L.F.; et al. Interaction of Copper(II) with Ditopic Pyridyl-*β*-diketone Ligands: Dimeric, Framework, and Metallogel Structures. *Cryst. Growth Des.* **2011**, *11*, 1697–1704. [CrossRef]

35. Kołodziejski, M.; Walczak, A.; Hnatejko, Z.; Harrowfield, J.; Stefankiewicz, A.R. Unsymmetrical bidentate ligands as a basis for construction of ambidentate ligands for functional materials: Properties of 4,4-dimethyl-1-phenylpentane-1,3-dionate. *Polyhedron* **2017**, *137*, 270–277. [CrossRef]

36. Gilli, P.; Pretto, L.; Bertolasi, V.; Gilli, G. Predicting Hydrogen-Bond Strengths from Acid−Base Molecular Properties. The pK_a Slide Rule: Toward the Solution of a Long-Lasting Problem. *Acc. Chem. Res.* **2009**, *42*, 33–44. [CrossRef]

37. Gimenez-Marques, M.; Calvo Galve, N.; Palomino, M.; Valencia, S.; Rey, F.; Sastre, G.; Vitorica-Yrezabal, I.J.; Jimenez-Ruiz, M.; Rodriguez-Velamazan, J.A.; Gonzalez, M.A.; et al. Gas confinement in compartmentalized coordination polymers for highly selective sorption. *Chem. Sci.* **2017**, *8*, 3109–3120. [CrossRef]

38. Brock, A.J.; Whittaker, J.J.; Powell, J.A.; Pfrunder, M.C.; Grosjean, A.; Parsons, S.; McMurtrie, J.C.; Clegg, J.K. Elastically Flexible Crystals have Disparate Mechanisms of Molecular Movement Induced by Strain and Heat. *Angew. Chem. Int. Ed.* **2018**, *57*, 11325–11328. [CrossRef]

39. Worthy, A.; Grosjean, A.; Pfrunder, M.C.; Xu, Y.; Yan, C.; Edwards, G.; Clegg, J.K.; McMurtrie, J.C. Atomic resolution of structural changes in elastic crystals of copper(II) acetylacetonate. *Nat. Chem.* **2018**, *10*, 65–69. [CrossRef]

40. Gould, J.A.; Athwal, H.S.; Blake, A.J.; Lewis, W.; Hubberstey, P.; Champness, N.R.; Schröder, M. Gas adsorption and structural diversity in a family of Cu(II) pyridyl-isophthalate metal–organic framework materials. *Philos. T. R. Soc. A* **2017**, *375*, 20160334. [CrossRef]

41. Liu, Y.; Zhao, Y.; Liu, Z.-Q.; Liu, X.-H.; Zhang, X.-D.; Sun, W.-Y. Coordination polymers with salicylaldehyde ligands: Structural diversity, selective sorption and luminescence sensing properties. *CrystEngComm* **2020**, *22*, 304–310. [CrossRef]

42. Zeng, M.-H.; Hu, S.; Chen, Q.; Xie, G.; Shuai, Q.; Gao, S.-L.; Tang, L.-Y. Apical Ligand Substitution, Shape Recognition, Vapor-Adsorption Phenomenon, and Microcalorimetry for a Pillared Bilayer Porous Framework That Shrinks or Expands in Crystal-to-Crystal Manners upon Change in the Cobalt(II) Coordination Environment. *Inorg. Chem.* **2009**, *48*, 7070–7079. [CrossRef] [PubMed]

43. Kanoo, P.; Mostafa, G.; Matsuda, R.; Kitagawa, S.; Kumar Maji, T. A pillared-bilayer porous coordination polymer with a 1D channel and a 2D interlayer space, showing unique gas and vapor sorption. *Chem. Commun.* **2011**, *47*, 8106–8108. [CrossRef] [PubMed]

44. Zeng, M.-H.; Feng, X.-L.; Chen, X.-M. Crystal-to-crystal transformations of a microporous metal–organic laminated framework triggered by guest exchange, dehydration and readsorption. *Dalton Trans.* **2004**, 2217–2223. [CrossRef] [PubMed]

45. Dolomanov, O.V.; Bourhis, L.J.; Gildea, R.J.; Howard, J.A.K.; Puschmann, H. *OLEX2*: A complete structure solution, refinement and analysis program. *J. Appl. Crystallogr.* **2009**, *42*, 339–341. [CrossRef]

46. Sheldrick, G.M. *SHELXT* – Integrated space-group and crystal-structure determination. *Acta Crystallographica A* **2015**, *71*, 3–8. [CrossRef]

47. Sheldrick, G.M. Crystal structure refinement with *SHELXL. Acta Crystallographica C* **2015**, *71*, 3–8. [CrossRef]

48. Agilent. *CrysAlis PRO*; Agilent Technologies Ltd and O: Yarnton, UK, 2014.

49. Oxford Diffraction. *CrysAlis RED*; Oxford Diffraction Ltd: Oxfordshire, UK, 2006.